Journal of Catalysis **208,** 83–88 (2002)
doi:10.1006/jcat.2002.3536, available online at http://www.idealibrary.com on IDEAL®

Evolution of Extraframework Iron Species in Fe Silicalite

2. Effect of Steaming

A. M. Ferretti,* C. Oliva,* L. Forni,* G. Berlier,† A. Zecchina,†,[1] and C. Lamberti‡

*Dipartimento di Chimica Fisica ed Elettrochimica, Università di Milano, Via C. Golgi 19, 20133 Milan, Italy; †Dipartimento di Chimica Inorganica, Fisica e dei Materiali, Università di Torino, Via P. Giuria 7, I-10125 Turin, Italy; ‡Dipartimento di Chimica Inorganica, Fisica e dei Materiali, Università di Torino, Via P. Giuria 7, I-10125 Torino, Italy; and INFM UdR di Università di Torino, Via P. Giuria 7, I-10125 Turin, Italy

Received July 30, 2001; revised November 21, 2001; accepted November 26, 2001

In the first part of this investigation, we studied in detail the structure, the oxidation state, and the mutual interconversion of extraframework iron species formed in Fe silicalite samples upon migration of iron from framework to extraframework positions induced by thermal activation and redox treatments. In this second part, we used temperature-dependent EPR, UV–vis, and IR spectroscopies to investigate the nature of the extraframework iron species present in Fe silicalite after steaming. Relatively large (≅30 nm) particles of iron oxide were detected. These large clusters are located outside the zeolite pores and are believed not to participate in partial oxidation reactions. It is shown that the Fe species which contribute to the formation of Fe_2O_3 extralattice particles are preferentially clustered grafted Fe^{2+} species. In contrast, isolated Fe^{2+} species are less affected by the steaming treatment. This suggests that the oxygen species active in the selective partial oxidation of benzene are adsorbed on isolated extraframework grafted Fe^{2+} centers. This result is of primary importance for the understanding of the structure of the oxygen species active in partial selective oxidation using N_2O as oxidant.

Key Words: **Fe silicalite; extraframework iron; benzene hydroxylation; steaming treatment; EPR; IR.**

1. INTRODUCTION

In recent years, a remarkable number of scientific works concerning iron-containing MFI systems have appeared. These materials have shown the best performance as catalysts for the direct oxidation of benzene to phenol with N_2O as oxidant (1, 2). Currently, the most widely used industrial route to phenol is the cumene process, in which cumene hydroperoxide undergoes an acid-catalyzed cleavage to phenol and acetone. The one-step process for the synthesis of phenol, using Fe silicalite as catalyst and generating N_2 instead of acetone as a side product, is obviously highly preferred (3). This explains the large number of studies devoted to the characterization of Fe–MFI materials, to the understanding of their catalytic activity, and in particular to the elucidation of the nature of the active sites.

It is widely accepted that the sites active in partial oxidation reactions are extraframework iron species (4–7). These species are formed inside the zeolite channels upon migration of Fe^{3+} from tetrahedral framework positions as a consequence of thermal treatments during catalyst activation (8–12). Successive thermal treatments at higher temperature are used to increase the number of extraframework active species and thus the catalytic activity in benzene to phenol reactions (8, 13, 14). In the first part of this work (12), we used IR, XANES, and EPR spectroscopies, to study the coordination and the oxidation state of extraframework species before, during, and after interaction with several probe molecules (CO, N_2O, and NO). This approach was applied to samples characterized by different iron content, activation temperature, and redox treatments. This allowed us to shed light on the structure, oxidation state, and mutual interconversion of a very complex family of extraframework iron species. This work has shown that migration of iron from isomorphously substituted Fe–MFI catalysts can guarantee a rather good dispersion of Fe inside the zeolitic walls and channels. Isolated and clustered grafted Fe^{3+} and Fe^{2+} species were detected, even in very highly diluted samples (Si/Fe = 150) (12), representing a true catalyst.

It was recently reported that mild steaming treatments, in comparison to vacuum treatments, resulted in better catalytic activity for Fe–ZSM-5 zeolites (15, 16). Steam treatment is known to modify the zeolite structure by favoring the breaking of Si–O–T bonds, where T = Al or Fe. It has been hypothesized that, after such a treatment, a considerable part of the extraframework iron species exits from the pore framework and forms Fe-containing agglomerates of high nuclearity (13). These agglomerates are too large to find room in the zeolitic pore network; thus, they are assumed to play no role in the benzene hydroxylation

[1] To whom correspondence should be addressed. Fax: 39-011-6707855. E-mail: adriano.zecchina@unito.it.

0021-9517/02 $35.00

reaction. However, the characterization of steamed catalysts is far from being completed.

In this work, we describe the results of an investigation, carried out on a steamed catalyst, designed to discriminate which catalytic active center(s) is (are) present in Fe–MFI systems among the heterogeneous variety of isolated, clustered, and grafted Fe^{3+} or Fe^{2+} species detected in Ref. (12). The choice of steamed catalysts is justified by the fact that they are still as active as, or even more active than, the original sample. This means that at least a fraction of the active sites must still be present in the form of highly dispersed centers inside the MFI channels. In other words, the steaming process seems to simplify the catalyst structure by eliminating the Fe species which are not (or are less) active in the oxidation process. This implies that the characterization of steamed samples must be done with care, to distinguish contributions coming from oxidic Fe particles segregated outside the zeolite crystals from those of the catalytic active sites still located inside the MFI pores.

2. EXPERIMENTAL

This work focuses on the Fe silicalite catalyst prepared by the hydrothermal method (17) labeled as FeS90 and described in detail in Ref. (12). Steaming treatment was performed in a flow of a mixture of 75 mol% steam in nitrogen at 773 K for 6 h, as described elsewhere (18). After this treatment, the color of the catalyst turned from white to light brownish; we shall refer to this catalyst as $FeS90_{st}$. Further recalcination at 823 K yields sample $FeS90_{recal}$.

The structural peculiarities of the FeS90 and $FeS90_{st}$ catalysts have been thoroughly investigated in previous papers (18, 19) and are only briefly summarized here. The FeS90 sample exhibits a BET surface area of ca. 350 m^2/g with total and micropore pore volumes of ca. 0.16 and 0.15 cm^3/g, respectively. Both porosity and surface area slightly increased in the steamed sample (19). XRD analysis guaranteed the absence of reflections different from those of the MFI structure. SEM micrographs showed that the crystal shape and size (0.5–1.0 μm) were maintained after steaming. The Fe concentration was 1.00 ± 0.04 wt% and remained constant after steaming. The $FeS90_{st}$ catalyst showed a selectivity to phenol (near 100 mol%) which was better than that of the FeS90 catalyst (19). Less systematic investigations were performed on the other samples described in Ref. (12).

Diffuse reflectance UV–vis spectra were obtained on a Varian Cary 5 spectrometer. A temperature-dependent EPR study was made on an X-band Bruker ELEXSYS E 500 instrument equipped with a cryogenic unit. The spectra were obtained on the thermally treated and steamed sample in the presence of air as described previously. As water vapor is not excluded, these samples must be considered as being in a hydrated state. The pressure (P_{NO})-dependent IR experiments were carried out at room temperature on a Bruker IFS 66 FTIR instrument as described in Ref. (12).

3. RESULTS AND DISCUSSION

3.1. The Effect of Steaming on the Clustering of Fe: Temperature-Dependent EPR Study

The lineshape variations of the EPR spectra as a function of temperature are reported in Fig. 1 for FeS90, $FeS90_{st}$, and $FeS90_{recal}$ (parts a, b, and c respectively). The EPR spectra observed with the "as-prepared" sample (Fig. 1a) seem more intense than those recorded after the following treatments (Figs. 1b and 1c). However, a quantitative measurement of this decreasing intensity is hazardous. Indeed, a reliable internal reference standard in each sample would be necessary for such an evaluation. Furthermore, the baseline is not perfectly flat, so affecting the result of any spectral integration. The spectra of the three catalysts are composed of three groups of lines localized in the $g \cong 2$, $\cong 3$, and $\cong 4$ spectral regions. Furthermore, in the $FeS90_{st}$ spectrum measured in the $90 < T < 130$ K interval, some narrow lines at a magnetic field $>5000\,G$ indicate the presence of physisorbed molecular O_2 (20). At each temperature, recalcination in He results in narrowing of the EPR lines. This might be explained by the dipolar interaction between O_2 and other paramagnetic species.

The expected line broadening with increasing temperature (due to the effect of the reticular vibrations on the spin relaxation) is observed for FeS90 (Fig. 1a). In contrast, a line narrowing with increasing temperature (accompanied by a symmetry increase of the lineshape) is observed for the $g \cong 2$ component for both $FeS90_{st}$ and $FeS90_{recal}$ samples (Figs. 1b and 1c). After recalcination, the EPR spectra are characterized by both an intensity inversion for the $g \cong 2$ and $g \cong 4.3$ components and the appearance of several unresolved features in the $g \cong 4.3$ region.

Line narrowing with increasing temperature, assuming a more symmetric Lorentzian shape, was attributed to the

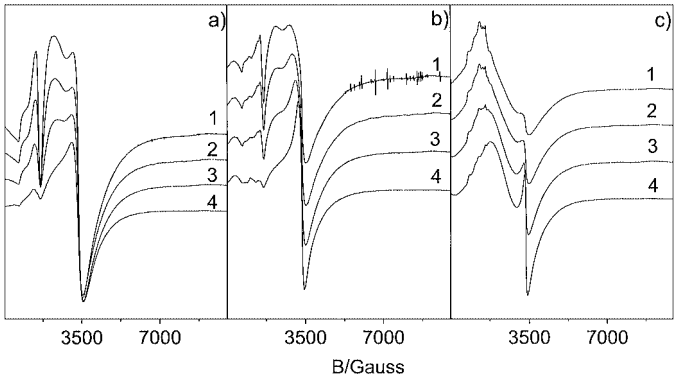

FIG. 1. Temperature-dependent (110, 150, 200, and 295 K curves 1–4). EPR study on spectra of FeS90, $FeS90_{st}$, and $FeS90_{recal}$, (parts (a), (b), and (c), respectively).

formation of superparamagnetic (single-domain) particles (21, 22). This phenomenon occurs when the temperature is high enough to average the magnetic anisotropy of the sample. A peak-to-peak linear broadening versus $1/T$ is then expected. A similar behavior was reported for both a series of oxide glasses containing highly dispersed nanoclusters of magnetite (23) and FeOOH nanoparticles (24). This behavior was also considered compatible with the formation of superparamagnetic particles up to 17 nm in size. A parallel situation was also reported for ultrafine Fe_3O_4 particles in ferrofluids (25). In this case, the presence of a nearly symmetric line was interpreted in terms of superparamagnetic interactions in Fe_3O_4 particles, characterized by a superparamagnetic relaxation time (τ_{sp}) shorter than the Larmor precession time (τ_L) within the magnetic resonance field H_0. τ_{sp} is related to the thermal fluctuation of the magnetic moment in single-domain particles smaller than a "critical size." For such particles (25), when the anisotropy energy is much smaller than kT the following relations hold (25),

$$\tau_{sp} \cong M_S V/(\gamma_0 kT) \quad \gamma_0 = 2\pi/(\tau_L H_0), \qquad [1]$$

where M_S is the saturation magnetization, V is the volume of the particle, γ_0 is the gyromagnetic ratio, and k is Boltzmann's constant. If the temperature is so high that $\tau_{sp} < \tau_L$, the magnetic anisotropies are "motionally" averaged out, and the EPR line narrowing is explained by the temperature-dependent factor, for example,

$$f \cong \tau_{sp}/\tau_L \cong M_S V H_0/(2\pi kT). \qquad [2]$$

When the volume distribution of the particles significantly covers the values ranging between the diameter of a single-domain particle (<15–20 nm) and the dimension of a superparamagnetic assembly of atoms (≅1 nm), the coexistence of ferrimagnetic and superparamagnetic systems is expected (26). The former causes a broader EPR feature, the latter a motionally narrowed one. Of course the interplay between the two phenomena can depend *inter alia* on the sample preparation method, the former being favored at a higher annealing temperature (21).

In the regime of motional narrowing the EPR linewidth should be expressed by

$$\Delta H = \alpha + \beta/T, \qquad [3]$$

where $\alpha = \Delta H_0$ is the linewidth for $T \to \infty$, $\beta = \Delta H_0 \gamma V \cdot V$ is the volume of the superparamagnetic particle undergoing fast relaxation and

$$\gamma = M_S H_0/(2\pi \mu_0 k), \qquad [4]$$

where M_S is the saturation magnetization value, H_0 is the resonance magnetic field in tesla ($1T = 10^4$ G), and $\mu_0 = 4\pi \times 10^{-7}$ Wb $A^{-1}m^{-1}$ is the vacuum permeability.

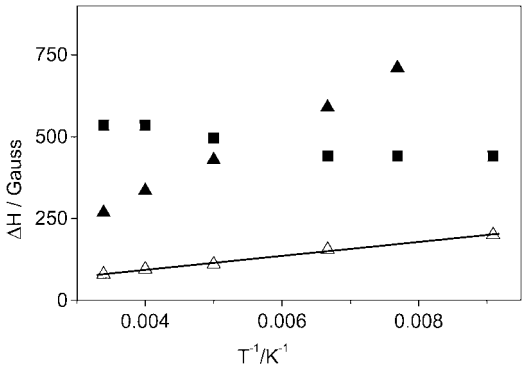

FIG. 2. Peak-to-peak EPR linewidth of FeS90 (■), $FeS90_{st}$ (▲), and $FeS90_{recal}$ (△) samples vs temperature. The solid line represents the linear interpolation of the set of data coming from $FeS90_{recal}$, where the model described in Eqs. [3]–[5] can be applied.

μ_0 must be introduced if M_S is expressed in tesla (as usual) instead of in A m^{-1}. According to Ref. (22), a value of 0.048 T is assumed for M_S, resulting, from Eq. [1], in $\gamma = 1.4 \times 10^{26}$ K m^{-3}.

The experimental ΔH plotted as a function of $1/T$ is reported in Fig. 2. Unfortunately this method can not be applied to the $FeS90_{st}$ data due to an additional broadening effect caused by the presence of adsorbed O_2 (20), *vide supra*. For $FeS90_{recal}$, the linear interpolation of the data leads to an evaluation of α and β, as seen in Eq. [3]: $\alpha = 8.1249$ G and $\beta = 21{,}294$ G K. The volume (V) of the superparamagnetic particles can thus be calculated as

$$V = \beta/(\alpha\gamma). \qquad [5]$$

A value of $V \approx 2\ 10^4$ nm^3 is obtained for sample $FeS90_{recal}$, resulting in a linear dimension of the superparamagnetic particles on the order of 30 nm. Smaller particles could also be present, contributing to the wings of the EPR spectra. The standard error on β (900 G K) implies that only the presence of superparamagnetic particles with a diameter greater than about 10 nm can be analyzed by this procedure. In conclusion, the data in Fig. 1c can be explained by the presence of particles with a diameter of around 30 nm, located in extracrystalline positions.

As the fraction of coordinatively unsaturated surface Fe sites present on particles of such dimensions is less than 5%, a decrease in catalyst activity is expected after steaming. As this does not occur, extralattice particles should be formed preferentially by clustering the Fe atoms coming from nonactive species.

3.2. The Effect of Steaming on the IR Spectra of Adsorbed NO

In Ref. (12), we employed the IR spectroscopy of adsorbed NO to investigate the nature of the extraframework iron species formed upon classical thermal treatments. The

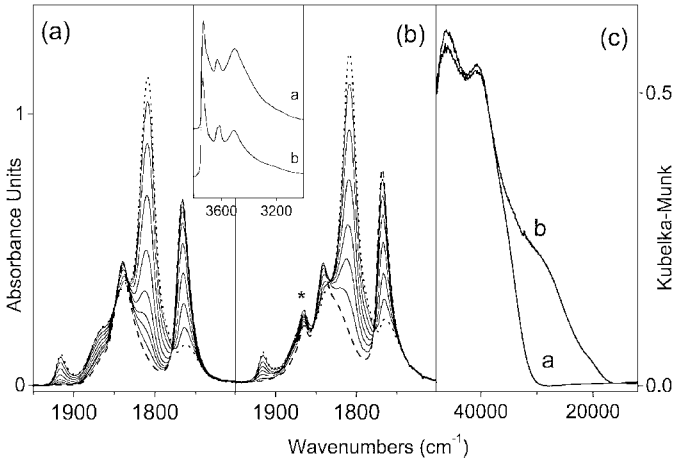

FIG. 3. Effect of steaming on sample FeS90 activated at 773 K. (a), (b) IR spectra of NO dosed at room temperature (decreasing P_{NO} from 15 Torr, dotted-line spectrum, to 10^{-3} Torr, dashed-line spectrum) on samples FeS90 and $FeS90_{st}$, respectively. (c) UV–vis spectra of FeS90 and $FeS90_{st}$ (curves a and b, respectively). The inset indicates the IR spectra, in the OH stretching region, of FeS90 and $FeS90_{st}$ (curves a and b, respectively).

species generated upon migration of iron were Fe^{3+} and Fe^{2+} ions grafted to the inner zeolite surface. Both isolated and bidimensionally clustered Fe^{2+} were detected. The structure of the Fe^{2+} species is heterogeneous and can be described as $L_2N_nFe^{2+}$, where L is a framework SiO^- (or the atomic O^{2-}) chemically linked group and N is a framework oxygen atom, electrostatically linked, of the vicinal SiOSi bridges. Depending on the number of N ligands, the Fe^{2+} species can adsorb 1, 2, or 3 NO with the formation of well-defined nitrosyl species.

This scheme (12) fully explains the spectra collected at increasing doses of NO adsorbed on FeS90 outgassed at 773 K (Fig. 3a). The complex spectra contain four main bands grouped into two pairs: the first one (1916, 1810 cm^{-1}) is ascribed to $L_2NFe^{2+}(NO)_3$ complexes; the second one (1835, 1765 cm^{-1}) to $L_2NFe^{2+}(NO)_2$ complexes (10, 12). The former transforms into the latter with decreasing P_{NO}. These Fe species are characterized by a high coordinative unsaturation and have been classified as isolated ferrous centers. Moreover, a second ferrous species contributes to the IR spectra reported in Fig. 3a (12). This species, when probed with NO, gives only the mononitrosyl $L_2N_3Fe^{2+}(NO)$ complex absorbing in the same region as the high-frequency component of the $L_2NFe^{2+}(NO)_2$ complexes ($\approx$1835 cm^{-1}). Unlike isolated species, this Fe^{2+} species does not show any propensity toward further NO uptake with increasing P_{NO}, reflecting a lower coordinative unsaturation. $L_2N_3Fe^{2+}$ species have thus been classified as "bidimensionally clustered" species, containing both extraframework and framework iron. Due to dipolar interaction, the $L_2N_3Fe^{2+}(NO)$ nitrosyl species formed upon NO contact are not EPR active (12). Conversely, IR spectroscopy of adsorbed NO is able to give information on both isolated and clustered iron species. Following the systematic procedure illustrated in (12), a steaming effect on samples FeS25, FeS50, and FeS50 has also been studied.

The IR spectra of NO adsorbed at room temperature on sample $FeS90_{st}$ (Fig. 3b) are not described in detail, as the observed spectra are basically similar to those registered before steaming (Fig. 3a). However, some differences can be observed. First, the steaming treatment did not appreciably reduce the IR features associated to nitrosyl complexes formed on isolated ferrous L_2NFe^{2+} species (doublets at 1916, 1810 cm^{-1} and 1835, 1765 cm^{-1}). This means that the steaming procedure has no effect on the species which appeared to be very resistant to H_2O (10, 12). Second, steaming modified the ratio between the 1835- and 1765-cm^{-1} components of the $L_2NFe^{2+}(NO)_2$ complexes. From the $I_{\nu 1765}/I_{\nu 1835}$ ratio at $P_{NO} = 15$ Torr, we obtain 1.58 and 1.82 before and after steaming, respectively. This means that after steaming the $L_2N_3Fe^{2+}(NO)$ complex formed on clustered Fe species, absorbing at around 1835 cm^{-1}, was significantly reduced. Third, a new IR feature was observed at 1865 cm^{-1} (labeled $*$ in Fig. 3b), which is ascribed to $Fe^{3+}(NO)$ adducts formed at the surface of the large Fe_2O_3 aggregates formed outside the zeolite crystals upon steaming. This assignment is supported by the fact that a similar band has already been observed on Fe silicalite samples with high iron loading, where clustering processes are expected (see Fig. 6d of Ref. (12)). The intensity of the 1865-cm^{-1} band increases with increasing activation temperatures (spectra not reported) as expected for clustered Fe^{3+} species. The relatively low intensity of the 1865-cm^{-1} band is in agreement with the rather large size of the Fe_2O_3 clusters revealed by the EPR measurements.

As a final observation, the inset in Fig. 3 indicates the variation of the IR spectrum, in the O–H stretching region, of the FeS90 catalyst upon steaming. Steaming affects the intensity of the 3720- and 3500-cm^{-1} bands attributed to free and hydrogen-bonded silanol groups in internal nests (27). This result indicates that steaming is likely associated with the decrease of internal defects. The band at 3630 cm^{-1}, with a shoulder at 3615 cm^{-1}, ascribed to Brønsted Fe(OH)Si groups, is modified by steaming with an apparent decrease of the 3630-cm^{-1} component. We think that this decrement is mainly a consequence instead of a real reduction of the decrease of the band at 3720 cm^{-1}.

The results discussed previously appear quite relevant because they indicate that (i) Fe species forming bidimensional paths ($L_2N_3Fe^{2+}$ species) are preferentially affected by steaming and (ii) isolated species are more resistant to the steaming procedure. As indicated in the literature, steamed samples are thought to be more active and selective in partial oxidation reactions (15, 16, 19). This seems to imply that the Fe species active in partial oxidation reactions are isolated. This conclusion can shed some light on

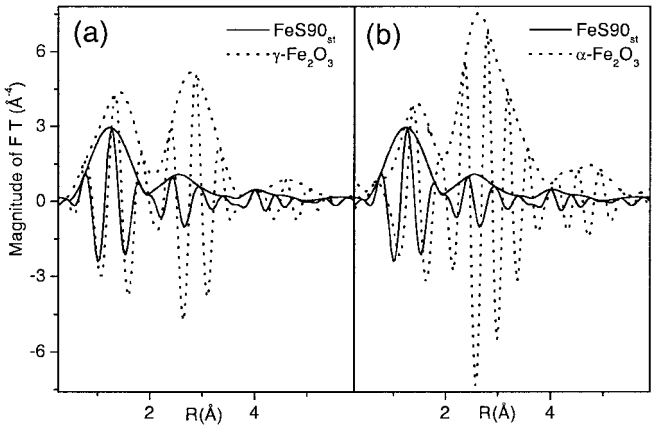

FIG. 4. (a) k^3-weighted, phase-uncorrected Fourier transform (modulus and imaginary part) done, in the interval 2.8–10.0 Å^{-1}, on the EXAFS spectrum of FeS90$_{st}$ catalyst (solid lines) and of γ-Fe_2O_3 model compound (dotted lines). (b) Comparison with α-Fe_2O_3 model compound.

the so-called α-oxygen species active in partial oxidation reactions. In fact, the view that α-oxygen is an oxygen species bridging pair of Fe atoms in a vicinal position (4, 5) seems to be weakened by these results. This does not indicate that oxygen adsorbed on bidimensionally clustered species is inactive in oxidation reactions; it simply suggests that it is less selective.

3.3. The Effect of Steaming on the UV–Vis Spectra

If the hypothesis advanced previously about the formation of Fe_2O_3 particles is correct, this should clearly be reflected in a variation of the UV–vis spectrum upon steaming, because the isolated and clustered species have distinctly different spectra. The changes induced by the steaming treatment on the UV–vis spectra of the FeS90 catalysts are reported in Fig. 3c. The spectrum of the light brown steamed sample shows, on the tail of the CT adsorption at around 30,000 cm^{-1} characteristic of isolated species (28), a new broad and complex adsorption in the range 30,000–18,000 cm^{-1}. This adsorption is due to small Fe_2O_3 clusters (8). This observation, together with the small decrement of the bands at $\nu > 30{,}000$ cm^{-1}, confirms beyond any doubt that steaming is associated with pronounced clustering.

4. CONCLUSIONS

The comparison of EPR and UV–vis results in "as prepared" and steamed samples evidences the formation of iron oxide particles upon steaming. EPR spectra suggest that these particles have an average diameter of around 30 nm and that they are thus located outside the zeolitic pores. This hypothesis is supported by the new band observed at 1865 cm^{-1} in the IR spectra of NO adsorbed on the steamed catalyst, which is ascribed to Fe^{3+}(NO) adducts formed at the surface of the large Fe_2O_3 aggregates. Of great relevance is the IR evidence, obtained by using NO as probe, that steaming does not appreciably affect the concentration of isolated ferrous L_2NFe^{2+} species while the bidimensionally clustered Fe species grafted to the internal surface are strongly reduced. This suggests that isolated iron species are the sites responsible for the selective oxidation of benzene to phenol.

ACKNOWLEDGMENT

The financial aid of the Italian Ministry of University and Scientific and Technological Research (MURST) through the COFIN 1998–2000 program is gratefully acknowledged.

Note added in proof. After the submission of our manuscript, we obtained new beamtime at the GILDA BM8 beamline of the ESRF where steamed Fe-silicalite was measured. The experimental set-up was the same adopted in the previous experiment, so we refer to the experimental section of Ref. (12).

Figure 4 reports the k^3-weighted, phase-uncorrected Fourier transform (modulus and imaginary part) done on the EXAFS spectrum of the FeS90$_{st}$ catalyst in the interval 2.8–10.0 Å^{-1}. For comparison, the FT of γ-Fe_2O_3 and α-Fe_2O_3 model compounds, performed in the same interval, are reported in parts (a) and (b), respectively. From the reported data, a second shell, absent before steaming (see Fig. 1 of Ref. (12)), is clearly emerging in the range where Fe–Fe contributions are expected in Fe_2O_3. Comparison with the same data measured for γ-Fe_2O_3 and α-Fe_2O_3 model compounds indicates that the imaginary part of the signal obtained from the catalyst is in fair agreement with that of γ-Fe_2O_3. This evidence well reflects the small and disordered nature of the oxidic nanoclusters formed on the catalyst after steaming and indirectly detected by UV–vis spectroscopy and temperature-dependent ERP study.

REFERENCES

1. (a) Gubelmann, M., and Tirel, P. J., Fr. Patent 2,630,735, 1988; (b) Kharitonov, A. S., Alexandrova, T. N. L., Vostrikova, A., Ione, K. G., and Panov, G. I., Russ. Patent 4,445,646, 1988.
2. Suzuki, E., Nakashiro, K., and Ono, Y., *Chem. Lett.*, 953 (1988).
3. Notté, P. P., *Top. Catal.* **13**, 387 (2000).
4. Sobolev, V. I., Panov, G. I., Kharitonov, A. S., Romannikov, V. N., Volodin, A. M., and Ione, K. G., *J. Catal.* **139**, 435 (1993).
5. Vodolin, A. M., Sobolev, V. I., and Zhidomirov, G. M., *Kinet. Katal.* **39**, 775 (1998).
6. Dubkov, A., Ovanesyan, N. S., Shteinman, A. A., Dubkov, K. A., Sobolev, V. I., and Panov, G. I., *Kinet. Katal.* **39**, 792 (1998).
7. Fejes, P., Nagy, J. B., Halász, J., and Oszkó, A., *Appl. Catal.* **61**, 85 (1990).
8. Bordiga, S., Buzzoni, R., Geobaldo, F., Lamberti, C., Giamello, E., Zecchina, A., Leofanti, G., Petrini, G., Tozzola, G., and Vlaic, G., *J. Catal.* **158**, 486 (1996).
9. Zecchina, A., Geobaldo, F., Lamberti, C., Bordiga, S., Turnes Palomino, G., and Otero Areán, C., *Catal. Lett.* **42**, 25 (1996).
10. Spoto, G., Zecchina, A., Berlier, G., Bordiga, S., Clerici, M. G., and Basini, L., *J. Mol. Catal. A* **158**, 107 (2000).
11. (a) Fejes, P., Nagy, J. B., Halász, J., and Oszkó, A., *Appl. Catal. A* **175**, 89 (1998); (b) Fejes, P., Nagy, J. B., Lázár, K., and Halász, J., *Appl. Catal. A* **190**, 117 (2000).
12. Berlier, G., Spoto, G., Bordiga, S., Ricchiardi, G., Fisicaro, P., Zecchina, A., Rossetti, I., Selli, E., Forni, L., Giamello, E., and Lamberti, C., *J. Catal.* **208**, 64 (2002).

13. Ribera, A., Arends, I. W. C. E., de Vries, S., Pérez-Ramírez, J., and Sheldon, R. A., *J. Catal.* **195**, 287 (2000).
14. Sobolev, V. I., Dubkov, K. A., Paukshtis, E. A., Pirutko, L. V., Rodkin, M. A., Kharitonov, A. S., and Panov, G. I., *Appl. Catal. A* **141**, 185 (1996).
15. Kharitonov, A. S., Panov, G. I., Sheleveva, G. A., Pirutko, L. V., Voskresenskaya, T. P., and Sobolev, V. I., U.S. Patent 5.672.777 (1996).
16. (a) PCT WO 95/27560, 19 Oct. 1995, to Boreskov Inst. of Catalysis, Novosibirsk, Russia; (b) Deut. Offen. DE 196 34 406 A1, 26 Aug. 1996, to Hoechst AG; (c) PCT WO 98/07513, 26 Feb. 1998, to Monsanto Co.; (d) PCT WO 98/07516, 26 Feb. 1998, to Monsanto Co.; (e) U.S. Patent 5,874,646, Feb. 23, 1999, to Solutia Inc.
17. Ratnasamy, P., and Kumar, R., *Catal. Today* **9**, 329 (1991).
18. Selli, E., Isernia, A., and Forni, L., *Phys. Chem. Chem. Phys*. **2**, 3301 (2000).
19. Leanza, R., Rossetti, I., Mazzola, I., and Forni, L., *Appl. Catal. A* **205**, 93 (2001).
20. Beringer, R., and Castle, J. G., *Phys. Rev.* **81**, 82 (1951).
21. Berger, R., Kliava, J., and Bissey, J.-C., *J. Appl. Phys*. **87**, 7389 (2000).
22. (a) "A.I.P. Handbook," Sect. 5g, 1963; (b) "Landolt-Bornstein," Vol. 2, pt. 9, 6th ed., 1962.
23. Ibrahim, M. M., Edwards, G., and Seehra, M. S., *J. Appl. Phys*. **75**, 5873 (1994).
24. Hagiwara, M., and Nagata, K., *J. Phys. Soc. Jpn.* **67**, 3590 (1998).
25. Sharma, V. K., and Waldner, F., *J. Appl. Phys*. **48**, 4298 (1977).
26. Cannas, C., Gatteschi, D., Musinu, A., Piccaluga, G., and Sangregorio, C., *J. Phys. Chem*. **102**, 7721 (1998).
27. Bordiga, S., Ugliengo, P., Damin, A., Lamberti, C., Spoto, G., Zecchina, A., Spanò, G., Buzzoni, R., Dalloro, L., and Rivetti, F., *Top. Catal.* **15**, 43 (2001).
28. Patarin, J., Tuilier, M. H., Durr, J., and Kessler, H., *Zeolites* **12**, 70 (1992).